Analysis of Puff Dynamics in Oocytes: Interdependence of Puff Amplitude and Interpuff Interval

Daniel Fraiman,* Bernardo Pando,* Sheila Dargan,† Ian Parker,† and Silvina Ponce Dawson*
*Departamento de Física, Facultad de Ciencias Exactas y Naturales, Universidad de Buenos Aires, Ciudad Universitaria, Buenos Aires, Argentina; and †Department of Neurobiology and Behavior, University of California, Irvine, California

ABSTRACT Puffs are localized Ca^{2+} signals that arise in oocytes in response to inositol 1,4,5-trisphosphate (IP_3). They are analogous to the sparks of myocytes and are believed to be the result of the liberation of Ca^{2+} from the endoplasmic reticulum through the coordinated opening of IP_3 receptor/channels clustered at a functional release site. In this article, we analyze sequences of puffs that occur at the same site to help elucidate the mechanisms underlying puff dynamics. In particular, we show a dependence of the interpuff time on the amplitude of the preceding puff, and of the amplitude of the following puff on the preceding interval. These relationships can be accounted for by an inhibitory role of the Ca^{2+} that is liberated during puffs. We construct a stochastic model for a cluster of IP_3 receptor/channels that quantitatively replicates the observed behavior, and we determine that the characteristic time for a channel to escape from the inhibitory state is of the order of seconds.

INTRODUCTION

The inositol 1,4,5-trisphosphate (IP_3) receptor (IP_3R) is a ligand-gated intracellular Ca^{2+} release channel that plays a central role in modulating cytoplasmic Ca^{2+} concentration and provides a link between cell surface receptors and Ca^{2+} release from intracellular stores. In addition to their regulation by IP_3, IP_3Rs show a biphasic modulation by cytosolic Ca^{2+}; for relatively low [Ca^{2+}] the channel open probability increases with [Ca^{2+}], whereas it reduces at high [Ca^{2+}] (1–5).

The spatiotemporal properties of signals arising through IP_3Rs have been extensively characterized by optical imaging in *Xenopus laevis* oocytes (6). These studies have revealed a hierarchical organization of release events, ranging from [Ca^{2+}] liberation from single IP_3Rs (''blips''), through the concerted opening of several IP_3Rs within a cluster (''puffs'') to global waves involving cluster-cluster interactions via [Ca^{2+}]-induced [Ca^{2+}] liberation (7). Puffs have also been observed in many other cell types (8–11), and appear to represent ubiquitous ''elementary events'' of intracellular [Ca^{2+}] signaling, which can have local signaling functions in their own right and also serve as building blocks from which global signals are constructed.

It is therefore important to understand the mechanisms underlying the generation and modulation of puffs. However, several aspects of puff dynamics still await clarification; most importantly, the mechanisms of puff termination and subsequent recovery of excitability. Given that Ca^{2+} is both a ligand of the IP_3R that affects its open probability and is the main ion carrier that flows through its pore, the Ca^{2+} ions that are released in the cytosol during a puff are expected to modulate the dynamics of a puff. Ca^{2+} release through a single IP_3R in a cluster may thus induce the regenerative opening of neighboring channels, which subsequently close because of the inhibitory effect of high local Ca^{2+} levels attained during the puff. Additional processes, however, may also affect puff termination, including the local depletion of luminal Ca^{2+} (an effect that is present in the case of sparks (12,13)) and the effect of counterions (14).

In this article, we examine the effects of cytosolic Ca^{2+} on puff dynamics by investigating the distributions of intervals between successive puffs occurring at a given site. Experimental data were obtained by fluorescence imaging of puffs evoked in *Xenopus laevis* oocytes by continuous photorelease of IP_3, and were analyzed to look for correlations between puff amplitudes and interpuff intervals. We find strong dependences between puff size and interpuff interval that can be explained in terms of an inhibitory role of Ca^{2+} binding to a cytosolic site on the IP_3R. Furthermore, by analyzing a simple model that reproduces the observed distributions we determine that the characteristic time for Ca^{2+} binding to this site is of the order of seconds.

MATERIALS AND METHODS

Experimental procedure

Preparation of Xenopus oocytes

Xenopus laevis were anesthetized by immersion in 0.17% MS-222 for 15 min and sacrificed by decapitation in adherence with protocols approved by the University of California, Irvine, Institutional Animal Care and Use Committee. Oocytes (stage V–VI) were manually plucked and collagenase-treated (0.5 $mg.ml^{-1}$ for 30 min) before storage in Barth's solution (composition in mM: 88 NaCl, 1 KCl, 2.4 $NaHCO_3$, 0.82 $MgSO_4$, 0.33 $Ca(NO_3)_2$, 0.41 $CaCl_2$, and 5 HEPES, pH 7.4) containing 0.1 $mg.ml^{-1}$ gentamicin at 17°C for 1–7 days before use. Intracellular microinjections were performed using a Drummond microinjector to load oocytes with

Submitted October 13, 2005, and accepted for publication February 10, 2006.

Address reprint requests to Daniel Fraiman, Depto. de Física, Facultad de Ciencias Exactas y Naturales, Universidad de Buenos Aires, Ciudad Universitaria, Pabellón I (1428), Buenos Aires, Argentina. E-mail: dfraiman@df.uba.ar.

0006-3495/06/06/3897/11 $2.00

doi: 10.1529/biophysj.105.075911

Oregon green 488 BAPTA 1 together with caged IP_3 (D-myo-inositol 1,4,5-trisphosphate, $P_{4(5)}$-(1-(2-nitrophenyl)ethyl) ester), and EGTA to respective final intracellular concentrations of 40, 4, and 270 μM, assuming a 1-μl cytosolic volume.

Confocal laser scanning microscopy

Confocal Ca^{2+} images were obtained using a custom-built line-scan confocal scanner interfaced to an Olympus IX70 inverted microscope (15). Recordings were made at room temperature, imaging in the animal hemisphere of oocytes bathed in normal Ringer's solution (composition in mM: 120 $NaCl_2$, 2 KCl, 1.8 $CaCl_2$, and 5 HEPES, pH 7.3). The laser spot of a 488-nm argon ion laser was focused with a 40× oil immersion objective (NA 1.35) and scanned every 8 ms along a 100-μm line. Emitted fluorescence was detected at wavelengths >510 nm through a confocal pinhole providing lateral and axial resolutions of ~0.3 and 0.5 μm, respectively. The scan line was focused at the level of the pigment granules and images were collected through a coverglass forming the base of the recording chamber. IP_3 was photoreleased from a caged precursor by delivering ultraviolet (UV) light, focused uniformly throughout a 200-μm spot surrounding the image scan line. After imaging resting fluorescence for 2 s, the UV light was kept on continually throughout the remainder of the recording (1 min), with the rate of photorelease of IP_3 controlled by a continuously variable neutral density filter.

Data processing and pooling

Fig. 1 *A* shows a typical experimental record in which the fluorescence ratio changes, $\Delta F(x,t)/F_0$, are depicted using a color code on a time-space plot (t,x). Here $\Delta F(x,t) \equiv F(x,t) - F_0$ and $F_0 \equiv \langle F(x,t<0)\rangle_t$, where the average is performed at each spatial point, x, over a certain number (~50) of times before IP_3 photorelease. The relative fluorescence is used to compensate for local inhomogeneities of the oocyte or of the dye distribution (16). EGTA was added to the injection solution (270 μM final cytosolic concentration) to functionally uncouple Ca^{2+} release sites, resulting in discrete puffs without propagating Ca^{2+} waves (17). For example, the line scan image in Fig. 1 *A* illustrates puffs generated at numerous sites, and Fig. 1 *B* shows the corresponding fluorescence ratios measured at five sites. The fluorescence ratio is directly related to the amount of Ca^{2+}-bound dye, [CaD] (16), but owing to the restricted time and space resolution of the imaging system such records can only provide information on the average concentration over a finite volume. When the dye is not saturated (which is the case in these experiments: $\Delta F(x,t)/F_0 \ll$ maximal change of ~10 in saturating $[Ca^{2+}]$), the spatiotemporal distribution of [CaD] should correspond about linearly to free Ca^{2+}.

Analyses were done on fluorescence profiles like those in Fig. 1 *B* from 46 different puff sites. We computed the local temporal average and the standard deviation of the fluorescence signal at a site using windows of the order of 2 s (i.e., of the order of the interpuff time and much longer than a typical puff duration) and identified the onset of a puff when the instantaneous fluorescence ratio exceeded the average value of the corresponding window by three standard deviations. The amplitude of the event, A, was taken as the maximum fluorescence ratio ($\Delta F(x,t)/F_0$) during the puff.

Ideally, we would have liked to work with very long recordings showing many release events at the same site. However, that was impracticable because of movement artifacts and eventual rundown of puffs. Instead, we grouped data from different release sites; typically with ~13 events observed at a given site. Because of the wide variation in puff amplitudes between different sites (possibly reflecting differences in numbers of channels per cluster), we classified release sites according to the size of the largest event observed at each. Fig. 2 shows the maximum puff amplitudes recorded from each of the 46 sites analyzed. We arbitrarily defined two groups of ''small'' (*solid circles*) and ''large'' clusters (*crosses*), representing a compromise between size of the resultant data sets and ''homogeneity'' of the cluster properties. All analyses presented here were based on events from

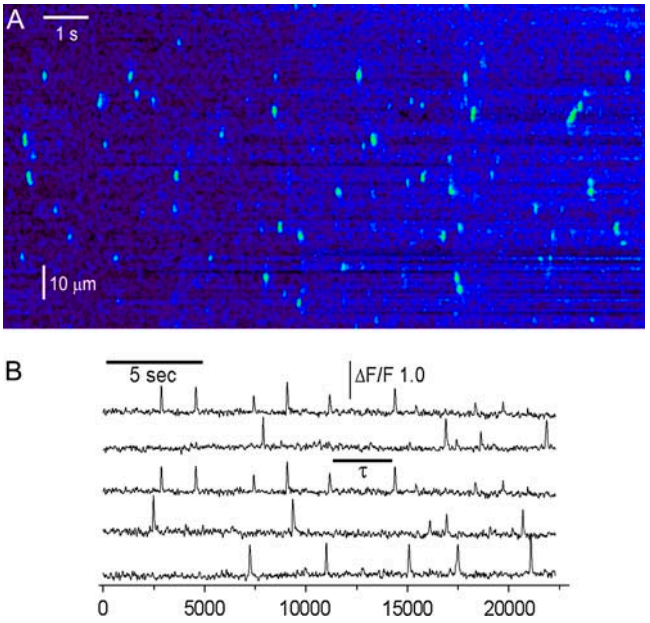

FIGURE 1 (*A*) Line scan image illustrating puffs evoked by sustained photorelease of IP_3. The y axis represents distance along the scan line, and time runs from left to right. Increases in fluorescence ratio ($\Delta F(x,t)/F_0$) are depicted on a pseudocolor scale, with ''warmer'' colors corresponding to increasing ratio (increasing free $[Ca^{2+}]$). The UV photolysis light was turned on ~10 s before the beginning of the record. (*B*) Traces show fluorescence profiles monitored from five of the puff sites in *A*. Solid line labeled ''τ'' illustrates the measurement of elapsed time between two successive puffs.

the small cluster group (18 release sites and 232 puffs). Similar results regarding the dependence between puff amplitude and interpuff times were obtained when the analysis was restricted to the group of large clusters (see Table 1).

Statistical tests and parameter fitting

Results are presented as frequency histograms of occurrence of certain subsets of events (e.g., puffs with amplitude within a certain range, etc.). The corresponding distribution of frequencies of the variable of interest (e.g., amplitude or interpuff time), $P_n(x)$, was used to compute the (cumulative) empirical distribution function, $F(X) = \int_{-\infty}^{X} dx P_n(x)$. To compare two

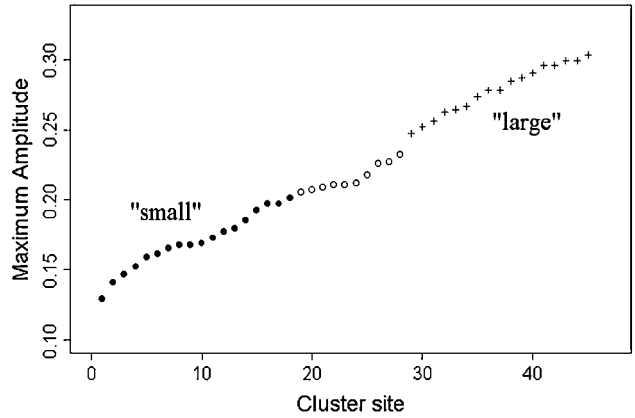

FIGURE 2 Maximum puff amplitude at each site.

TABLE 1 Kolmogorov test for the conditional distributions of the group of large clusters

	A_n/τ_{n-1}	τ_n/A_n
17%	$T = 0.511$, $p < 0.001$	$T = 0.316$, $p = 0.023$
25%	$T = 0.437$, $p < 0.001$	$T = 0.303$, $p = 0.004$
50%	$T = 0.274$, $p < 0.001$	$T = 0.237$, $p = 0.002$

The group of large clusters is represented by crosses in Fig. 2.

stochastic processes, we compare the distribution functions of some of the stochastic variables that characterize the processes. In the case of the experiments, it is the empirical distribution function that is obtained from the variable of interest. In the case of the model we analyze in this article, we compute it as in the experimental case, using the results that come from extensive numerical simulations of the stochastic process. Once we have two distribution functions that we wish to compare, F_1 and F_2, we compute the Kolmogorov statistics,

$$T \equiv \sup_x |F_1(x) - F_2(x)|. \quad (1)$$

Statistical significance (p-values) of differences between distributions was determined from look-up tables (18).

In this article, we present a stochastic model that reproduces the experimental observations. To determine parameter values for the model, we initially divided the parameter space using a relatively coarse grid, performed stochastic simulations for each set of parameter values in the grid and computed the cumulative distribution function, F_{sim}, for the interpuff time. This was compared with the experimentally determined one, F_{exp}, and the initial parameter values were rejected if a Kolomogorov test determined that the simulated and experimental values were different ($p < 0.05$). Once we attained a subset of parameter values for which F_{sim} and F_{exp} were not significantly different, we refined the grid of parameter values and iteratively repeated this procedure.

RESULTS

Analysis of experimental data

Fig. 3 shows histograms of puff amplitude, A, and interpuff time, τ, for the set of events analyzed in this article (i.e., the set of small events defined in Fig. 2). The amplitude distribution is asymmetric and has a maximum around 0.1 with standard deviation, $\sigma = 0.032$. The interpuff time distribution resembles a log-normal or γ-distribution and has a maximum around 1.5 s with standard deviation, $\sigma = 1.37$ s. This distribution is similar to the one obtained in Yao et al. (6) using pooled data from three puff sites.

We analyze now the existence of dependencies between puff amplitude and interpuff time. A scatter plot of the amplitude of the nth event, A_n versus the time elapsed from the preceding event at the same site, $\tau_{n-1} \equiv t_n - t_{n-1}$ (with t_n the time at which the nth event occurs), did not reveal any structure (data not shown). However, various conditional distributions do display differences, reflecting the existence of dependences between puff amplitude and interpuff time. We show in Fig. 4 the distributions of event amplitudes, A_n, grouped according to whether the elapsed time from the previous event at the same site, τ_{n-1}, was smaller than the first quantile, q_1, of the interpuff time distribution (Fig. 4 *A*, $\tau_{n-1} < q_1 = 1.4$ s) or larger than the third quantile, q_3 (Fig. 4 *B*, $\tau_{n-1} > q_3 = 3.27$ s). The conditional distributions are different: for smallτ_{n-1} values, the next puff, on average, has a smaller amplitude than for large values of τ_{n-1}.

Fig. 5 shows the corresponding distributions of interpuff times, $\tau_n = t_{n+1} - t_n$, conditional on whether the amplitude of the preceding puff, A_n, was small ($A_n < q_1 = 0.092$) or large ($A_n > q_3 = 0.134$). We again observe differences in both distributions: for small A_n, the distribution of intervals after those puffs clusters around $\tau_n \sim 1$ s, whereas for large A_n the distribution peaks near $\tau_n \sim 3$ s and has a larger dispersion.

To further explore the relationships between puff amplitude and interpuff time, we computed the corresponding conditional distribution functions, using two different definitions of large and small previous interpuff time, τ_{n-1} or amplitude, A_n. Namely, we first included in the sets of small or large interpuff times, τ_{n-1}, only the 17% with the smallest values and the 17% with the largest values, respectively. We show the distribution functions of subsequent amplitudes, A_n, obtained in this way in Fig. 6 *A* (curve *1* for the set of small previous interpuff times, τ_{n-1}, and curve *4* for the set of large previous interpuff times). The total number of events is 40 for each set in this case. We then divided the total set of previous interpuff times in two halves, with 50% of the data (116 events) in each set. We show the corresponding distribution functions of subsequent amplitudes in Fig. 6 *A* (curve *2* for the new set of small previous interpuff times and curve *3* for the new set of large previous interpuff times). A similar analysis was done for the cumulative distribution function of interpuff times, τ_n (Fig. 6 *B*). These data show that the amplitude (interpuff time) distributions conditioned to large or small previous interpuff times (amplitudes) are

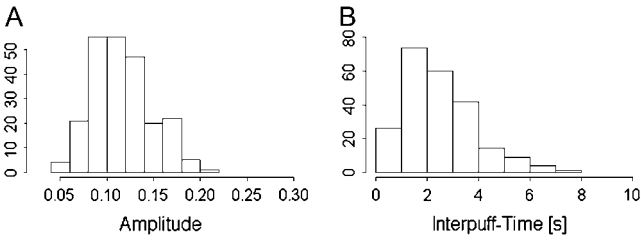

FIGURE 3 Histograms of puff amplitude A (*A*) and interpuff time τ (*B*).

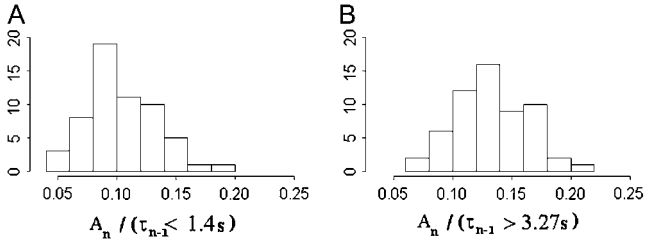

FIGURE 4 Puff amplitude (A_n) histogram conditional to (*A*) $\tau_{n-1} < 1.4$ s and (*B*) $\tau_{n-1} > 3.27$ s. The differences in the distribution functions are statistically significant ($p < 0.001$).

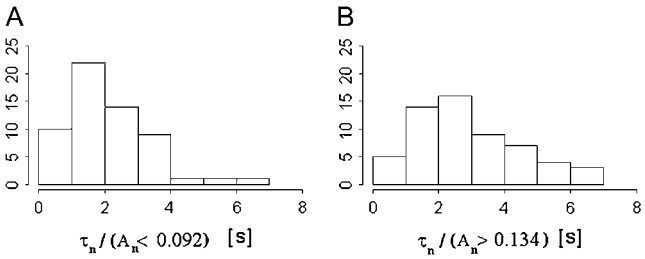

FIGURE 5 Interpuff time (τ_n) histogram conditional to (*A*) $A_n < 0.092$ and (*B*) $A_n > 0.134$. The differences in the distribution functions are statistically significant ($p < 0.04$).

different, and that the differences are more pronounced as the maximum interpuff time (amplitude) value in the set of small times (amplitudes) becomes more different from the minimum interpuff time (amplitude) value in the set of large values.

Table 1 summarizes the dependencies between puff amplitude and interpuff times obtained for the group of large clusters (Fig. 2, *crosses*). In this case, the equal distribution hypothesis is always rejected.

Mechanisms underlying correlated puff behavior

The results of Figs. 3 and 4 reveal an inhibitory effect after a puff. Namely, interpuff intervals tend to be longer after large puffs; and puffs tend to be smaller after short intervals. Several possible mechanisms may underlie these correlations. One is that the high cytosolic [Ca^{2+}] attained during a puff inhibits channels within the cluster, so that the amplitude and probability of occurrence of a subsequent puff recover with a time course reflecting the recovery of channels from an inhibited state. Other processes that might affect the interpuff time include local depletion of Ca^{2+} in the endoplasmic reticulum (ER) lumen leading to decreased single-channel current (19) and/or affecting the channel open probability (20); or the effect of counterions that might affect Ca^{2+} dynamics on both the cytosolic and luminal sides (14,21). Under our experimental conditions, we expect local luminal [Ca^{2+}] depletion to be small (see, e.g., Callamaras and Parker (17), Thul and Falcke (19), and Shuai and Parker (22)). In this article, we therefore explore whether the observed behavior can be accounted for by an inhibitory effect of the cytosolic [Ca^{2+}] on the channels within a cluster.

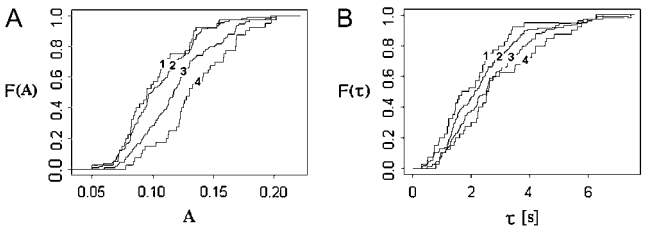

FIGURE 6 (*A*) Conditional amplitude distribution function for the sets of small previous interpuff times, τ_{n-1}, containing the 17% (curve *1*) and 50% smallest values (curve *2*) of τ_{n-1} and for the set of large previous interpuff times containing the 17% (curve *4*) and 50% largest values (curve *3*) of τ_{n-1}. In both cases, the differences in the distribution functions are statistically significant ($p < 0.002$). (*B*) Similar to *A*, but for the interpuff time distribution function conditional to small or large values of the previous puff amplitude, A_n. The various curves correspond to the sets containing the 17% smallest (curve *1*), the 50% smallest (curve *2*), the 17% largest (curve *4*), and the 50% largest (curve *3*) values of A_n. The Kolmogorov test gives *p*-values of 0.04 comparing curves 1 and 3, and 0.18 comparing curves 2 and 4.

An idealized model in terms of individual channels

We developed an idealized cluster model containing a finite number of channels, N, with IP_3 bound. Given that most of the time IP_3 is bound to its corresponding site, even for relatively low values of [IP_3] (see Discussion), for simplicity, we neglect fluctuations in N due to IP_3 binding and unbinding. That would only introduce some statistical noise. Each of these N channels can exist in two main states: inhibited or uninhibited. Uninhibited channels may be open (during a release event) or closed (during the interpuff time). Since we are interested in understanding the interpuff time distribution, not the kinetics of the puffs themselves, we assume that a release event (i.e., channel open time) is instantaneous. If a channel is in the inhibited state it has to wait a time that is exponentially distributed with mean value $1/\lambda_2$ to become uninhibited. An inhibited channel cannot open. An uninhibited channel opens with probability per unit time λ_1 if all the other channels of the cluster are closed, and opens with probability 1 if any other channel in the cluster opens; i.e., if one channel opens, calcium-induced calcium release causes all the uninhibited channels of the cluster to open simultaneously. Several assumptions are implicit in this model. First, a sudden increase in the local cytosolic [Ca^{2+}] induces channel opening of IP_3Rs with IP_3 bound before it can induce inhibition, in agreement with experimental data showing faster binding to activating site(s) on IP_3Rs than to inhibitory sites (see, e.g., Adkins and Taylor (23)). Second, the amount of Ca^{2+} released during a puff is enough to open all uninhibited channels of the cluster with IP_3 bound. This appears reasonable, given that the cytosolic [Ca^{2+}] averaged over the focal region around a cluster is of the order of 10 μM during a small puff (L. Bruno, Universidad de Buenos Aires, personal communication, 2005). The probability, λ_1, on the other hand, is related to the probability that the necessary ions bind to one channel in the cluster, inducing its opening. Clearly, this depends on the concentrations of agonists (IP_3 and Ca^{2+}), and although [IP_3] can be assumed to remain constant during the experiment, the cytosolic [Ca^{2+}] changes dramatically during a puff. We assume that cytosolic [Ca^{2+}] returns close to its basal level relatively soon after the puff ends (in part due to the presence of EGTA in the experiments we are looking at, which ''balkanizes'' Ca^{2+} signals (24)). Indeed, numerical simulations of how free cytosolic [Ca^{2+}] varies upon Ca^{2+} release from the ER

with a current of 0.05 pA show that $[Ca^{2+}]$ averaged over a 20-nm^3 region around the channel's mouth drops from ~40 μM to <100 nM in <1 ms after channel closure (G. Solovey, D. Fraiman, B. Pando, and S. Ponce Dawson, unpublished; see also Thul and Falcke (19)). This time is much shorter than the typical interpuff time. Thus, the assumption that the cytosolic $[Ca^{2+}]$ is around the basal level ($[Ca^{2+}] \sim$ 50 nM) between puffs is realistic. In the model, an uninhibited channel may become inhibited in a puff with a probability, p_{inh}, that depends on the number of channels that opened during the puff, N^o. This is equivalent to assuming that p_{inh} depends on the cytosolic $[Ca^{2+}]$ attained during a puff, which is an increasing function of N^o (19). The inhibition probability, p_{inh}, is a monotonically increasing function of N^o (and of $[Ca^{2+}]$) such that $p_{inh} \to 1$ as $N^o \to \infty$. To limit the number of free parameters, we consider the exponential function, $p_{inh}(N^o) = 1 - (1 - a) \times \exp(-(N^o - 1)b)$, where a and b are adjusted to match the experimental data. Similar results were obtained with a sigmoidal function (data not shown). The p_{inh} models the inhibitory effect of cytosolic Ca^{2+} on single IP_3Rs, which occurs with high probability for large enough $[Ca^{2+}]$. We show in Fig. 7 the system dynamics that apply when Ca^{2+} binding to an ''activating'' site is the rate-limiting process for opening of uninhibited channels. This assumption holds for the IP_3R if $[Ca^{2+}]$ is close to its basal value ($[Ca^{2+}] \sim 50$ nM), as we are assuming is the case between puffs.

We can relate the parameters λ_1, λ_2, a, and b of the model to properties of single IP_3Rs. Namely, λ_1 is the probability per unit time that the necessary number of Ca^{2+} ions binds to activating sites of an IP_3R with IP_3 bound and induce channel opening. Assuming that IP_3R inhibition is only due to the inhibiting effect of cytosolic Ca^{2+}, λ_2 is then the probability per unit time at which Ca^{2+} unbinds from the inhibiting site(s). Since we find that $1/\lambda_2$ is relatively large, which means that it takes a relatively long time for the channel to become uninhibited, we can assume that the function $p_{inh}(N^o)$ is mainly determined by the stationary open probability at the (high) cytosolic $[Ca^{2+}]$ that is achieved near the channel's mouth during a puff. Namely, we can assume that $1 - p_{inh}(N^o)$ provides an upper bound of this open probability, $P_o([Ca^{2+}]) \le 1 - p_{inh}(N^o) = (1 - a)\exp(-(N^o - 1)b)$, so that $1 - a \ge P_o([Ca^{2+}])$ and b^{-1} gives the rate at which P_o decreases with with N^o or, equivalently, with cytosolic $[Ca^{2+}]$ at the high concentrations that are reached during the puff (see Discussion).

Estimating the model parameters from the experimental data

We adjusted the parameters of the model to minimize the value of T defined in Eq. 1, with F_1 the (cumulative) distribution function of interpuff times obtained experimentally (displayed in Fig. 3 *B*) and F_2 that obtained from the model. Given that we are not using any of the conditional distributions shown in Figs. 4 and 5 to fit the parameters, the subsequent ability of the model to reproduce these conditional distributions serves as a validation of the model. This fitting procedure cannot provide the value of N. On the other hand, the values of λ_1 and λ_2 should be related to N (e.g., if we decrease N, we expect the fitted values of λ_1 to get larger to obtain the experimentally determined mean interpuff time). We could find N if we had a way to determine the relationship between puff amplitude, A, and the number of open channels, N^o. If we assume that the smallest events that we observe correspond to $N^o = 1$ and the largest ones to $N^o = N$ (for the type of cluster that we are analyzing) and that there is a linear relationship between A and N^o, then we could estimate from Fig. 4 *A* that N (the number of channels with IP_3 bound) is ~4 or 5. This number coincides with the typical number of open channels in a puff estimated by Swillens et al. (26). However, it is not completely clear that the relationship between relative fluorescence (amplitude) and number of open channels should be linear (19). Therefore, we decided to repeat all the calculations for two values of N, $N = 4$ and $N = 16$.

For $N = 4$, the best parameter values that we find are $\lambda_1 = 0.225\ s^{-1}$, $\lambda_2 = 0.4\ s^{-1}$, $a = 0.8$, and $b = 1.8$, for which the test defined by Eq. 1 gives $T = 0.07$ ($p = 0.22$, i.e., the hypothesis that the two distributions are the same cannot be rejected). For $N = 16$, the best parameter values that we find are $\lambda_1 = 0.043\ s^{-1}$, $\lambda_2 = 0.67\ s^{-1}$, $a = 0.6$, and $b = 1.5$, for which the test defined by Eq. 1 gives $T = 0.08$ ($p = 0.11$). These parameter values are contrasted against single IP_3R properties in the Discussion section.

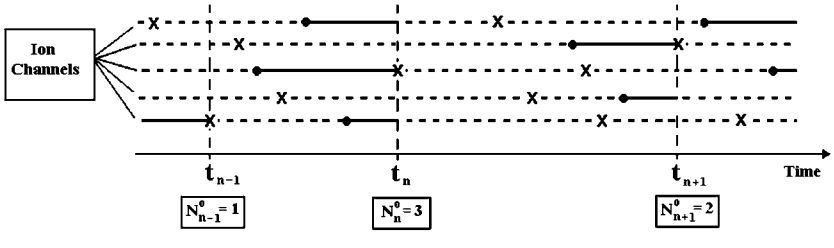

FIGURE 7 Simple model of cluster dynamics in terms of individual channels. Random binding events of Ca^{2+} ions to activating sites on IP_3R are marked by crosses. If the channel is inhibited (*dashed lines*), nothing happens. If the channel is uninhibited (*solid lines*), it opens, resulting in opening of all other uninhibited channels in the cluster to generate a puff. During each puff, some of the uninhibited channels become inhibited, with a probability that is a (saturating) increasing function of the puff amplitude (characterized by the number of channels that opened during the puff, N^o). At any time, an inhibited channel may spontaneously become uninhibited (*solid black circle*) with a probability per unit time of λ_2. The schematic illustrates a cluster of five channels, which generates three puffs involving varying numbers of open channels.

Model results

To check that the model in fact reproduces the interpuff time distribution that was used for the fitting and to test its ability to reproduce other features of the experimentally determined distributions not enforced with the fitting, we performed numerical simulations using $N = 4, \lambda_1 = 0.225\ s^{-1}, \lambda_2 = 0.4\ s^{-1}$, $a = 0.8$, and $b = 1.8$. We show in Fig. 8 the histograms of the number of open channels in a puff, N^o, and of the interpuff times, τ, obtained with these simulations. As expected, the τ distribution thus obtained is statistically indistinguishable from the experimental one (compare Figs. 8 *B* and 3 *B*)). The Kolmogorov statistic is $T = 0.07$, giving a p-value of 0.22 for the equal-distribution null hypothesis. A quantitative comparison of the N^o distribution and amplitude distribution histograms is not possible at this time because we do not know the relationship between puff amplitude and number of open channels.

We show in Fig. 9 the conditional distributions of the number of open channels for the sets of small ($\tau < 1.4$ s) and large ($\tau > 3.27$ s) previous interpuff times. Although we do not know the relationship between observed puff amplitude and number of open channels, the way the histograms change as we condition them to small (Fig. 9 *A*) or large (Fig. 9 *B*) previous interpuff times is qualitatively similar to the change observed experimentally and shown in Fig. 4.

We show in Fig. 10 the conditional distributions of interpuff times for the sets of small and large previous numbers of open channels, $N^o \leq 2$ and $N^o \geq 3$. Also in this case, the agreement with the observations of Fig. 5 is very good. Furthermore the Kolmogorov test does not reject the equal-distribution hypothesis between the simulated conditional distributions and the experimental ones ($p > 0.5$).

We repeated all these computations using $N = 16$. Also in this case, the test defined by Eq. 1 gives a reasonably good value ($p = 0.11$), for which the hypothesis that the interpuff time distribution functions obtained with the model and with the experiments are the same cannot be rejected. However, whereas three of the parameter values that we obtain with the fitting procedure are similar to the $N = 4$ case ($\lambda_2 = 0.67\ s^{-1}$, $a = 0.6$, and $b = 1.5$), the value of λ_1 ($0.043\ s^{-1}$) is harder to justify from the point of view of the single IP_3R dynamics. If

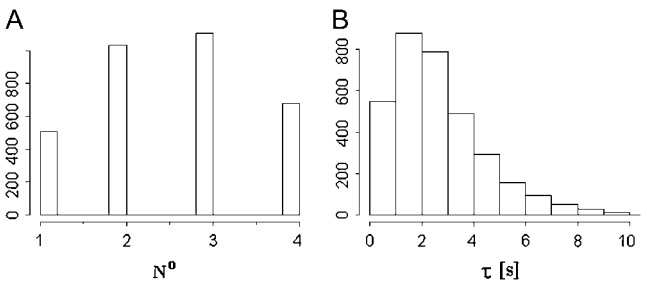

FIGURE 8 Histogram of the number of open channels during a puff (*A*) and of interpuff times (*B*) obtained from stochastic simulations of our model using $N = 4$, $\lambda_1 = 0.225\ s^{-1}$, $\lambda_2 = 0.4\ s^{-1}$, $a = 0.8$, and $b = 1.8$.

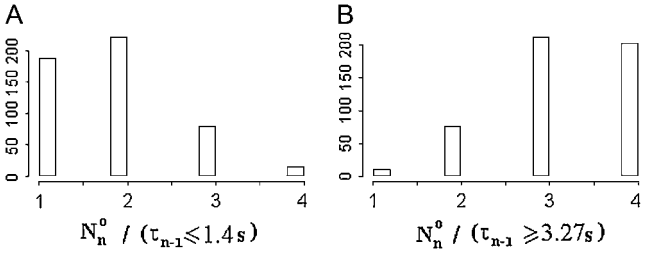

FIGURE 9 Histograms of open channels, with N^o conditional to small, $\tau_{n-1} < 1.4$ s (*A*), and large, $\tau_{n-1} > 3.27$ s (B), previous interpuff times.

we relate it to the rate of Ca^{2+} binding to n activating sites of the IP_3R in the absence of inhibition (see Discussion), using the rates of the DeYoung-Keizer model (23) we obtain $n = 7$, which is too large. On the other hand, although the various conditional distribution functions analyzed in this article are qualitatively similar to the experimentally determined ones, the Kolomogorov tests give p-values that are not as good as in the $N = 4$ case ($p = 0.022$ for the set of small previous amplitudes and $p = 0.094$ for the set of large previous amplitudes). For this reason, all subsequent results will be restricted to the $N = 4$ case.

Model predictions and suggested further tests

The simple model introduced in this article explains the experimentally observed distributions of puff amplitude and interpuff times in terms of the competition between two basic processes: inhibition and channel opening. The degree of inhibition is related to the amount of Ca^{2+} that is released during a puff and, at the single-channel level, the typical timescale of inhibition is given by $1/\lambda_2$. In the model, the opening of the first channel during a puff is triggered by random binding of Ca^{2+} at basal cytosolic [Ca^{2+}] levels with a typical timescale given by $1/\lambda_1$. The fitting of the previous section gives us $1/\lambda_1 > 1/\lambda_2$, which means that, typically, each channel becomes uninhibited faster than the rate at which it is challenged by basal Ca^{2+} to become open. Under the assumptions for which the model works, IP_3 enters mainly to determine the effective number of IP_3Rs in a cluster, N, that are amenable to make a transition to the open state (and contribute to a puff). This number does affect the statistics of the cluster as a whole. It is thus of interest to analyze how the mean puff amplitude and the mean interpuff times change when the balance between inhibition and channel opening is changed by a change in the rates at which they occur at the single-channel level, or by a change in the number of ''available'' IP_3Rs in a cluster.

To investigate how the various intervening factors affect puff dynamics, we performed numerical simulations keeping the same values as before for all parameters but one, and investigated how the mean number of open channels at a site during a puff, $\langle N^o \rangle$, and the mean interpuff time at the same

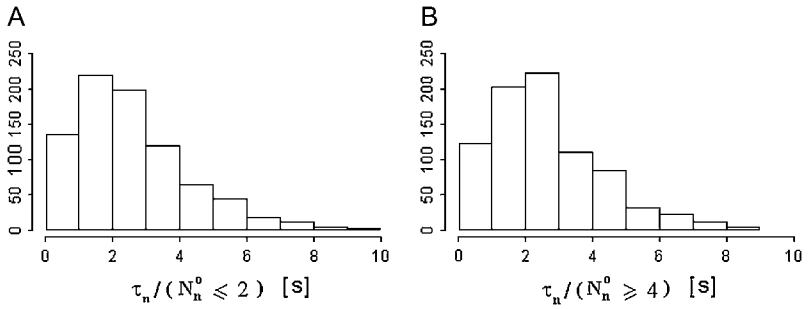

FIGURE 10 Conditional distributions of interpuff times, τ, for the set of small, $N^o \leq 2$ (*A*), and large, $N^o \geq 3$ (*B*) previous numbers of open channels.

site, $\langle\tau\rangle$, changed. We show in Figs. 11 *A* and 12 *A* the results obtained for $\lambda_1 = 0.225\ s^{-1}$, $\lambda_2 = 0.4\ s^{-1}$, $a = 0.8$, $b = 1.8$ and various values of N (2, 3, 4, 5, 6, 7, and 8). $N = 4$ corresponds to the case discussed in the previous section. We observe that $\langle\tau\rangle$ decreases and $\langle N^o\rangle$ increases when N, the number of IP_3Rs in the cluster with IP_3 bound, increases. Thus, $\langle\tau\rangle$ increases with $\langle N^o\rangle$ (as N increases), as shown in Fig. 12 *A*. Although we do not know the exact relationship between N^o and the observed puff amplitude, A, we do expect it to be an increasing function. Therefore, based on the results of Fig. 12 *A*, we expect the observed $\langle\tau\rangle$ to increase with $\langle A\rangle$ if this is either due to a larger amount of IP_3 or to a larger mean cluster size. In fact, if we compute the mean amplitude and interpuff time for the set of large clusters (defined in Fig. 2), we find that $\langle A\rangle$ is larger and that the mean and the median interpuff times (mean = 2.48 s, median = 2.26 s, $\sigma = 1.37$ s) are smaller than in the group of small clusters (mean = 2.36 s, median = 2.04 s, $\sigma = 1.37$ s). Although this result has the tendency predicted by Fig. 12 *A*, the numerical differences are not statistically significant.

In Figs. 11 *B* and 12 *B*, we show the dependence of mean interpuff time, $\langle\tau\rangle$ on λ_1 for $N = 4$, $\lambda_2 = 0.4\ s^{-1}$, $a = 0.8$, and $b = 1.8$. By increasing λ_1, we are increasing the frequency at which Ca^{2+} ions can bind to the IP_3R activating sites. Since channel opening also depends on whether the channel is inhibited or not, the net effect of increasing λ_1 will thus compete with the effect of inhibition, whose typical timescale is $1/\lambda_2$. We observe in Fig. 11 *B* that $\langle\tau\rangle$ decreases with λ_1, until it reaches a plateau that depends on the value of N. This is similar to the behavior of Fig. 11 *A*: increasing λ_1 increases the interpuff frequency, because IP_3Rs are challenged more often by the Ca^{2+} ions that are present in the cytosol between puffs. However, the behavior of $\langle N^o\rangle$ is different in Fig. 11, *A* and *B*. That is, $\langle N^o\rangle$ decreases with increasing λ_1, because as $1/\lambda_1$ becomes comparable with $1/\lambda_2$, the limiting process for the occurrence of a puff becomes inhibition rather than channel opening. Thus, very likely, when the first channel in a cluster opens, most of the other channels will be inhibited because not enough time has elapsed (compared with $1/\lambda_2$). Therefore, on average, events become smaller in size than when individual IP_3Rs are challenged less often (smaller λ_1). As a result, in this case, $\langle\tau\rangle$ is an increasing function of $\langle N^o\rangle$, as shown in Fig. 12 *B*).

We also tested the effects of changing the probability that an uninhibited channel becomes inhibited during the occurrence of a puff, $p_{inh}(N^o) = 1 - (1 - a) \times \exp(-(N^o - 1)b)$. In particular, we observed that if p_{inh} is increased, by increasing either a or b while leaving the other parameters fixed, the mean interpuff time, $\langle\tau\rangle$ increases. The mean number of open channels during a puff, $\langle N^o\rangle$, on the other hand, decreases when b is increased, but increases with a for $a < 0.3$ and then decreases (data not shown). The fact that $\langle\tau\rangle$ increases with p_{inh} is very intuitive, since a larger inhibition probability should lead to a larger mean interpuff time. As in the case of Fig. 12 *B*), the decreasing behavior of $\langle N^o\rangle$ with p_{inh} is related to the fact that inhibition becomes the limiting process for puff occurrence as p_{inh} becomes large enough.

DISCUSSION AND CONCLUSIONS

We have analyzed sequences of puffs observed using optical techniques in oocytes of *Xenopus laevis*. We show that there

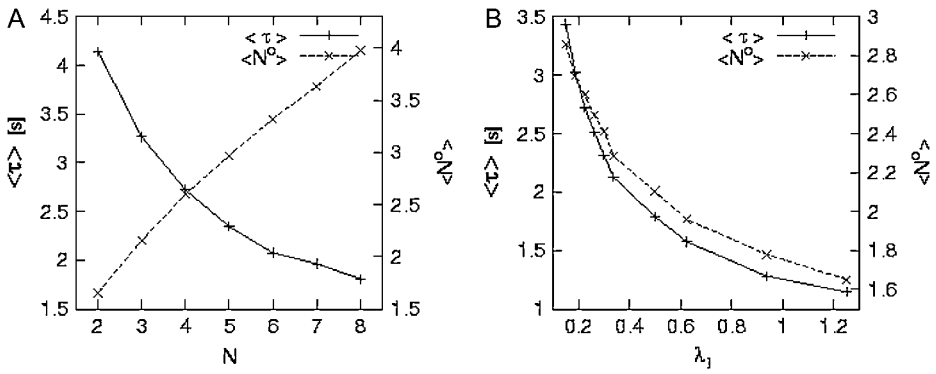

FIGURE 11 (*A*) Mean number of open channels during a puff, $\langle N^o\rangle$ (*crosses*) and mean interpuff time, $\langle\tau\rangle$ (*asterisks*) as a function of the number of functional channels in the cluster, N. (*B*) Mean number of open channels during a puff, $\langle N^o\rangle$ (*crosses*) and mean interpuff time, $\langle\tau\rangle$ (*asterisks*) as a function of the rate of Ca^{2+} binding to a channel in the cluster, λ_1.

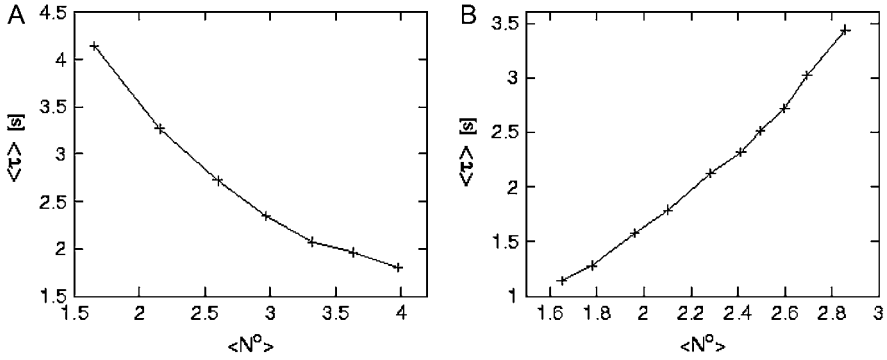

FIGURE 12 Mean interpuff time, $\langle\tau\rangle$, as a function of the mean number of open channels during a puff, $\langle N^{o}\rangle$ for $N = 2, 3, 4, 5, 6, 7$, and 8 (A), and for various values of λ_1 (*B*).

is a dependence between interpuff time and puff amplitude for puffs that occur at the same site (cluster of channels) in the oocyte. Namely, puffs of large amplitude are most likely followed by a long interpuff time. In addition, puffs that occur after a large interpuff time has elapsed are most likely large. We show the occurrence of this behavior in recordings containing relatively small puffs involving the release through very few channels (IP_3Rs) that was evoked by a permanent photorelease of IP_3. Given the small amplitude of the puffs, which we expect should result in a small local Ca^{2+} depletion on the luminal side, we investigated the possibility of explaining this behavior in terms of the inhibiting role that cytosolic Ca^{2+} can exert on IP_3Rs. To this end, we constructed a very simple stochastic model that yet retains the main features of clusters of IP_3Rs. The stochastic model reproduces the observed behavior quantitatively and provides some interesting predictions regarding the way the observed behavior would change by varying the Ca^{2+} basal concentration or $[IP_3]$.

The simple stochastic model of puff dynamics that we have introduced in this article is characterized by three probabilities that can be related to single IP_3R properties: λ_1, the probability per unit time that an IP_3R with IP_3 bound opens at basal Ca^{2+} levels; λ_2, the probability per unit time that an (inhibited) IP_3R loses the Ca^{2+} ions that induced its inhibition; $p_{inh}(N^{o})$, the probability that an IP_3R becomes inhibited during a puff. The model is also characterized by the maximum possible number of ''active'' IP_3Rs in the cluster, N (i.e., the number of IP_3Rs with IP_3 bound). We fixed a value of N and determined the values of the parameters that characterize the three probabilities by a fitting procedure. The most reasonable values of λ_1 and λ_2 were obtained for $N = 4$.

Assuming that the rate of Ca^{2+} binding to one activating site is k_{on}^{act} and that Ca^{2+} binding to n (independent) activating sites is needed to induce channel opening (provided that IP_3 is already bound and that there is no Ca^{2+} bound to the inhibitory sites of the channel), then we can relate λ_1 and k_{on}^{act} by $\lambda_1 \sim ([Ca^{2+}]/K_d)^{n-1} k_{on}^{act}[Ca^{2+}]$, where K_d is the dissociation constant of each (activating) Ca^{2+} binding site. The fitting procedure with $N = 4$ gave $\lambda_1 = 0.225\ s^{-1}$. This value is compatible with the one that obtained using models of the IP_3R for $[Ca^{2+}] = 50$ nM and $n > 1$. For example, if we use the DeYoung-Keizer model (27), we determine that for $n = 3$ it is $([Ca^{2+}]/K_d)^{n-1} k_{on}^{act}[Ca^{2+}] = 0.37\ s^{-1}$. If we repeat this calculation using the rate, λ_1, determined with the fitting with $N = 16$, $\lambda_1 = 0.043\ s^{-1}$, we obtain $n = 7$, which is too large.

The value of λ_2 obtained with the fitting with $N = 4$, $\lambda_2 = 0.4\ s^{-1}$, implies that the mean time that a channel remains inhibited is of the order of 2.5 s. This number is consistent with results of other experiments that were done to assess the inhibiting role of cytosolic Ca^{2+} on IP_3-evoked Ca^{2+} liberation (28). Ca^{2+} signals evoked by paired photorelease of IP_3 showed a maximal depression of the second response at a flash interval of ~1 s, and the response then recovered progressively as the interflash interval was lengthened (28). The time course of this recovery is consistent with our simple model. We assume that N_c clusters of IP_3Rs are observed and that each of them contains, on average, N uninhibited IP_3Rs at the time ($t = 0$) of the first IP_3 release. Neglecting the latency between IP_3 release and puff occurrence and the time differences at which the different puffs that constitute the signals occur, based on our model we assume that there are, on average, $N(1 - p_{inh}(N)\exp(-\lambda_2 t))$ uninhibited IP_3Rs in each cluster at the time, t, at which the second release of IP_3 occurs. Both the puff amplitude and the probability that a puff will be evoked at a given cluster are proportional to the number of uninhibited IP_3Rs. Thus, we expect the increment in fluorescence caused by the second signal, F_2, and the one caused by the first signal, F_1, to be related by $F_2/F_1 = (1 - p_{inh}(N)\exp(-\lambda_2 t))^2$. A nonlinear fit of the data in Fig. 7 of Parker and Ivorra (28) gives $\lambda_2 = 0.35 \pm 0.05\ s^{-1}$ (with a (0.25,0.50) 95% confidence interval). The value of λ_2 determined in this article ($0.4\ s^{-1}$) is within this confidence interval. This gives us more confidence about the number that we could extract from the experiments analyzed in this article using our simple model, i.e., a typical time of inhibition of the order of seconds.

Our model explains this behavior in terms of the inhibition that cytosolic Ca^{2+} exerts on individual IP_3Rs. However, an alternative explanation could be that the ER is partially depleted during a puff and that it takes a time of the order of a few seconds to be refilled. We think that this other explanation can be ruled out in the experiments we analyze in this

study. As argued before, we are working with puffs of very low amplitude so that the local ER depletion will be negligible (19). Furthermore, the experiments of Dargan and Parker (24), in which the addition of large amounts of BAPTA induced a prolonged release of Ca^{2+} from the ER, indicate that the inhibitory role of cytosolic Ca^{2+} is a key factor in determining puff duration. Thus, our estimate of λ_2 points to the existence of an inhibited state for the IP_3R induced by Ca^{2+} binding to a cytosolic site with a mean lifetime of the order of seconds. This result has implications for puff termination. According to these results, at the $[Ca^{2+}]$s that are reached during a puff, single IP_3Rs make a transition to an inhibited state whose mean lifetime is much larger than the typical duration of a puff. Therefore, Ca^{2+} inhibition may be the main reason for puff termination. This is also consistent with the effect of BAPTA, described before. Our estimated value of λ_2 also has implications for the kinetics of single IP_3Rs. Namely, if inhibition is due to Ca^{2+} binding to some cytosolic sites, $1/\lambda_2$ should provide a lower bound for the mean time that an IP_3R remains closed in single-channel experiments when cytosolic $[Ca^{2+}]$ is of the order of the values that it achieves during a puff (which we estimate as ~50–120 μM in an ~20 (nm^3) region around the channel's mouth). $1/\lambda_2 = 2.5$ s is much larger than the mean closed time reported in Mak et al. (29) for $[Ca^{2+}] = 100$ μM and $[IP_3] = 10$ μM with or without ATP. However, it could be compatible with the behavior at $[IP_3] = 33$ nM shown in this article (mean closed times at $[IP_3] = 33$ nM are shown up to $[Ca^{2+}] = 3$ μM only and they are of the order of 0.1 s (29)). It is compatible with the values of the model presented in Bezprozvanny and Ehrlich (30), in which the time for the recovery of IP_3Rs from Ca^{2+}-induced inactivation was estimated to be between 1.25 and 2.6 s. Similar conclusions can be obtained using the value of λ_2 determined with the fitting with $N = 16$ ($\lambda_2 = 0.67$ s^{-1}).

Given that the time it takes for a single inactivated IP_3R to become uninhibited (~2 s) is much longer than a typical puff duration (~0.05 s), p_{inh} is both the probability that a single active IP_3R will become inhibited during the time duration of a puff and that a fraction of active IP_3Rs will become inhibited during a puff. Given the relatively short duration of a puff, we expect p_{inh} to be smaller than the fraction of channels that are inhibited under a stationary condition of high $[Ca^{2+}]$, as the one achieved during a puff (50–120 μM). In fact, it can be proven that p_{inh} is smaller than the stationary value using the rate of $[Ca^{2+}]$ binding to the inhibitory site of the DeYoung-Keizer model and the rate of inhibition release that we obtain, λ_2. The stationary probability of a channel being inhibited, on the other hand, is smaller than the stationary probability of it being closed. Therefore, we can assume that $p_{inh} \leq 1 - P_o([Ca^{2+}])$, with $P_o([Ca^{2+}])$ the stationary open probability at $[Ca^{2+}] \sim$ 50–120 μM, from which we get that $P_o([Ca^{2+}]) \leq 1 - p_{inh}(N^o) = (1 - a)\exp(-(N^o - 1)b)$. Therefore, $1 - a$ is an upper bound for P_o at the cytosolic $[Ca^{2+}]$ that is reached when a single channel opens, whereas b^{-1} modulates the rate at which P_o decreases with cytosolic $[Ca^{2+}]$ (actually, with N^o). The parameters obtained with the fitting, $a = 0.8$ and $b = 1.8$, imply that the upper bound, $(1 - p_{inh})$, decreases from 0.2 (for $N^o = 1$) at a cytosolic concentration $[Ca^{2+}] \approx 40$ μM to 0.001 ($N^o = 4$) at $[Ca^{2+}]$ between 120 and 160 μM. These upper bounds are compatible with the observations of Bezprozvanny et al. (3) at $[IP_3] \leq 2$ μM and of Mak et al. (5) at $[IP_3] \leq 33$ nM. It is difficult to know the $[IP_3]$ during the experiments in which IP_3 is photoreleased; however, in Parker and Ivorra (31), the IP_3 concentration that evokes puffs was estimated to be between 50 and 100 nM. Based on this estimation, the model gives a stationary open probability upper bound compatible with observations in Bezprozvanny et al. (3). Nevertheless, we do not have conclusive evidence to say that the bound is not compatible with the observations in Mak et al. (5), since no $P_o([Ca^{2+}])$ curve has been reported for $[IP_3] = 50$ nM (for $[IP_3] = 100$ nM, the upper bound is smaller than $P_o([Ca^{2+}] = 40$ μM)). On the other hand, single IP_3R observations seem to be contradictory. However, we have suggested in a previous work (20) that one way to reconcile the observations of Bezprozvanny and co-workers (3) and Mak and co-workers (5) is to assume that single IP_3R open probability is modulated by luminal Ca^{2+}. If the local $[Ca^{2+}]$ on the luminal side does not vary much during the time course of each experiment (which is one of the assumptions of our model, given the small amplitude of the puffs we analyze), our simple model could then be used to assess the effect of luminal Ca^{2+} on single IP_3Rs. Similar conclusions can be obtained using the values of b and a determined for $N = 16$.

We also determined how the observed interpuff time distribution and mean number of open channels during a puff would change if some of the parameters of our model were changed. In trying to test these predictions experimentally, the greatest difficulty is introducing the necessary changes in a very controlled way so that the main assumptions of the model are not violated (if they are, we cannot guarantee that the conclusions still hold). In particular, we analyzed what could happen if the number of IP_3Rs with IP_3 bound increased. Increasing this number could be achieved by increasing the light intensity with which IP_3 is uncaged during the experiment. That would serve as long as waves are not induced or the average Ca^{2+} level between puffs does not increase too much compared with its basal value. We obtained that, in the model, the mean interpuff time, $\langle\tau\rangle$, decreased and the mean number of open channels during a puff, $\langle N^o\rangle$, increased with N. Based on these results, we concluded that $\langle\tau\rangle$ should increase with the mean puff amplitude $\langle A\rangle$ and this would occur both due to a larger amount of IP_3 or to a larger mean cluster size. In fact, we obtained some encouraging results by computing the mean puff amplitude and interpuff time for the set of large clusters, for which we obtained a larger $\langle A\rangle$ and a smaller $\langle\tau\rangle$ than for

the set of small clusters, although the differences were not statistically significant.

The fact that $1/\lambda_1 > 1/\lambda_2$ (a relation that we obtain from the fitting) means that, typically, each IP_3R becomes uninhibited faster than the rate at which it is challenged by basal Ca^{2+} to become open. We then used the model to investigate what its predictions were if we changed this inequality, namely, if λ_1 was increased leaving the other parameters fixed. We obtained that the mean interpuff time decreased, whereas the mean number of open channels during a puff decreased. The first observation is easy to understand: interpuff frequency increases with λ_1 because IP_3Rs are challenged more often to become open. The other observation is due to the competition between channel challenging by basal Ca^{2+} (characterized by λ_1) and channel inhibition (characterized by λ_2). Namely, as $1/\lambda_1$ becomes comparable with $1/\lambda_2$, the limiting process for the occurrence of a puff becomes inhibition rather than channel opening. Therefore, if $1/\lambda_1$ is too small, the opening of the first channel in a cluster cannot induce the opening of many others because most of them are still inhibited. In this way, events tend to be smaller in size than when λ_1 is smaller. Testing this prediction experimentally is not so easy, because it is hard to alter λ_1 individually. In principle, it could be done by changing the basal Ca^{2+} level; however, it cannot be done by increasing this level by large amounts. Namely, for the assumptions of the model to still hold, we need Ca^{2+} binding to the activating sites to be the limiting process for channel opening when channels are not inhibited (something that would be violated if the rates of Ca^{2+} and IP_3 binding become comparable) and we need Ca^{2+}-induced inhibition to be very rare at basal Ca^{2+} levels. Decreasing the basal $[Ca^{2+}]$, on the other hand, would not affect our assumptions. Therefore, one possibility would be the use of a slow buffer, like EGTA, that would not affect the values of $[Ca^{2+}]$ that could be attained around the channel's mouth during the opening of a single IP_3R, but that could alter the basal $[Ca^{2+}]$ level between puffs (varying λ_1). In fact, the use of moderate amounts of EGTA induces ''event potentiation'', i.e., an increment of puff amplitude, as reported by Dargan and Parker (24). It is not clear that this observed potentiation is related to a more likely release of inhibition between puffs due to a lower amount of basal Ca^{2+} determined by the presence of EGTA, mainly because the experimental observation corresponds to events that occur almost simultaneously at many sites. The use of EGTA, on the other hand, balkanizes Ca^{2+} signals (17), which can be related to the decrease of λ_1 that could result from a lower cytosolic $[Ca^{2+}]$ between puffs. Therefore, these two observations seem to fit within the dual role that we envisage for cytosolic Ca^{2+} in our model. The use of relatively large amounts of BAPTA in the experiments of Dargan and Parker (24), on the other hand, induce an almost permanent Ca^{2+} release from internal stores, where individual puffs cannot be distinguished. In principle, very large amounts of BAPTA could alter the distribution of cytosolic Ca^{2+} within the cluster, even when a single IP_3R is open. Therefore, the presence of BAPTA could not only change λ_1, but also decrease $p_{inh}(N^o)$ for each value of the number of open channels, N^o. Our model cannot describe a situation in which cytosolic Ca^{2+} does not go back to its basal value almost immediately after the occurrence of a puff. However, the fact that by decreasing p_{inh}, the mean interpuff time decreases is in accordance with the observation of an almost permanent release of Ca^{2+} in the presence of large amounts of BAPTA. The effect of assuming that single IP_3R inhibition by cytosolic Ca^{2+} is moderated (due to the presence of a fast buffer like BAPTA) should be similar to the effect of assuming that more channels with IP_3 bound are present in the cluster. In fact, we observe that, according to the model, both the mean interpuff frequency and the mean number of open channels during a puff increase with increasing N. Although not completely conclusive, an analysis of the subset of clusters that displayed the largest puff amplitudes indicates that this is indeed the case.

Even though simple, our model allows the extraction of single IP_3R information from the analysis of experiments in which several IP_3Rs work concordantly to generate a puff. In this respect, the existence of an inhibited state with mean time duration of the order of a few seconds is a feature that could be contrasted against mean closed times of single IP_3Rs, as we did before. Different values of mean closed times have been reported in the literature for the same amount of IP_3, which we interpreted in a previous work (20) as due to the use of diverse amounts of luminal Ca^{2+} in the various experiments. Mean closed times are also dependent on $[IP_3]$, which is a variable that is hard to know in optical experiments. If the assumption that luminal Ca^{2+} remains approximately constant during the time course of the experiments that we analyze is correct, then we can determine with which values of $[IP_3]$ and luminal $[Ca^{2+}]$ the parameters of our model are compatible. Thus, our model can help us build a comprehensive picture of single IP_3R dynamics. Although we think that luminal Ca^{2+} does not play a relevant role in the experiments we analyzed in this article, further investigations are necessary to draw a definite conclusion. This is particularly important in view of the observations indicating that luminal Ca^{2+} signals spark termination and determines the interspark refractory time in myocytes, a cell type in which Ca^{2+} release occurs through ryanodine receptors (12, 13). Although more experiments and analyses are necessary to arrive at a definite conclusion in the case of oocytes, we think that our approach sheds light on the elusive behavior of IP_3Rs in their native environment.

S.P.D. is a member of the Carrera del Investigador Científico (Consejo de Investigaciones Científicas y Técnicas).

This research was supported by Universidad de Buenos Aires, PICT 03-08133 of Agencia Nacional de Promoción Científica y Tecnológica (Argentina), and National Instituites of Health grant GM65830.

REFERENCES

1. Iino, M. 1990. Biphasic calcium dependence of inositol trisphosphate induced calcium release in smooth muscle cells of the guinea pig *Taenia caeci*. *J. Gen. Physiol.* 95:1103–1122.
2. Finch, E. A., T. J. Turner, and S. H. Goldin. 1991. Calcium as a co-agonist of inositol 1,4,5-trisphosphate-induced calcium release. *Science*. 252:443–446.
3. Bezprozvanny, I., J. Watras, and B. E. Ehrlich. 1991. Bell-shaped calcium-response of Ins(1,4,5)P3- and calcium-gated channels from endoplasmic reticulum of cerebellum. *Nature*. 351:751–754.
4. Ramos-Franco, J., M. Fill, and G. A. Mignery. 1998. Isoform-specific function of single inositol 1,4,5-trisphosphate receptor channels. *Biophys. J.* 75:834–839.
5. Mak, D. O., S. McBride, and J. K. Foskett. 1998. Inositol 1,4,5-trisphosphate activation of inositol trisphosphate receptor Ca^{2+} channel by ligand tuning of Ca^{2+} inhibition. *Proc. Natl. Acad. Sci. USA*. 95:15821–15825. Erratum in *Proc Natl Acad Sci USA*. 1999. 96:3330.
6. Yao, Y., J. Choi, and I. Parker. 1995. Quantal puffs of intracellular Ca2+ evoked by inositol trisphosphate in Xenopus oocytes. *J. Physiol.* 482:533–553.
7. Sun, X., N. Callamaras, J. S. Marchant, and I. Parker. 1998. A continuum of InsP3 -mediated elementary Ca2+ signalling events in *Xenopus* oocytes. *J. Physiol.* 509:67–80.
8. Thomas, D., P. Lipp, S. C. Tovey, M. J. Berridge, W. Li, R. Y. Tsien, and M. D. Bootman. 2000. Microscopic properties of elementary Ca^{2+} release sites in non-excitable cells. *Curr. Biol.* 10:8–15.
9. Melamed-Book, N., S. G. Kachalsky, I. Kaiserman, and R. Rahamimoff. 1999. Neuronal calcium sparks and intracellular calcium ''noise''. *Neurobiology*. 96:15217–15221.
10. Koizumi, S., M. D. Bootman, L. K. Bobanovic, M. J. Schell, M. J. Berridge, and P. Lipp. 1999. Characterisation of elementary Ca^{2+} release signals in NGF-differentiated PC12 cells and hippocampal neurones. *Neuron*. 22:125–137.
11. Huser, J., and L. A. Blatter. 1997. Elementary events of agonist-induced Ca^{2+} release in vascular endothelial cells. *Am. J. Physiol.* 42:C1775–C1782.
12. Terentyev, D., S. Viatchenko-Karpinski, H. H. Valdivia, A. L. Escobar, and S. Gyorke. 2002. Luminal Ca^{2+} controls termination and refractory behavior of Ca^{2+}-induced Ca^{2+} release in cardiac myocytes. *Circ. Res.* 91:414–420.
13. Szentesi, P., C. Pignier, M. Egger, E. G. Kranias, and E. Niggli. 2004. Sarcoplasmic reticulum Ca^{2+} refilling controls recovery from Ca^{2+}-induced Ca^{2+} release refractoriness in heart muscle. *Circ. Res.* 95: 807–813.
14. Nguyen, T., W.-C. Chin, and P. Verdugo. 1998. Role of Ca^{2+}/K^{+} ion exchange in intracellular storage and release of Ca^{2+}. *Nature*. 395: 908–912.
15. Parker, I., N. Callamaras, and W. G. Wier. 1997. A high-resolution, confocal laser scanning microscope and flash photolysis system for physiological suties. *Cell Calcium*. 21:441–452.
16. Ventura, A. C., L. Bruno, A. Demuro, I. Parker, and S. P. Dawson. 2005. A model-independent algorithm to derive Ca^{2+} fluxes underlying local cytosolic Ca^{2+} transients. *Biophys. J.* 88:2403–2421.
17. Callamaras, N., and I. Parker. 2000. Phasic characteristic of elementary Ca^{2+} release sites underlies quantal responses to IP_3. *EMBO J.* 19: 3608–3617.
18. Conover, W. C. Practical Nonparametric Statistics. Wiley, Hoboken, NJ.
19. Thul, R., and M. Falcke. 2004. Release currents of IP3 receptor channel clusters and concentration profiles. *Biophys. J.* 86:2660–2673.
20. Fraiman, D., and S. Ponce Dawson. 2004. A model of the IP3 receptor with a luminal calcium binding site: stochastic simulations and analysis. *Cell Calcium*. 35:403–413.
21. Marchant, J., and C. Taylor. 1998. Rapid activation and partial inactivation of inositol trisphosphate receptors by inositol trisphosphate. *Biochemistry*. 33:11524–11533.
22. Shuai, J., and I. Parker. 2005. Optical single-channel recording by imaging Ca^{2+} flux through individual ion channels: theoretical considerations and limits to resolution. *Cell Calcium*. 37:283–299.
23. Adkins, C. E., and C. W. Taylor. 1999. Lateral inhibition of inositol 1,4,5-trisphospate receptors by cytosolic Ca^{2+}. *Curr. Biol.* 9:1115–1118.
24. Dargan, S., and I. Parker. 2004. Buffer kinetics shape the spatiotemporal patterns of IP3-evoked Ca2+ signals. *J. Physiol.* 553: 775–788.
25. Reference deleted in proof.
26. Swillens, S., G. Dupont, L. Combettes, and P. Champell. 1999. From calcium blips to calcium puffs: theoretical analysis of the requirements for interchannel communication. *Proc. Natl. Acad. Sci. USA*. 96: 13750–13755.
27. De Young, G. W., and J. Keizer. 1992. A single-pool inositol 1,4,5-trisphosphate-receptor agonist-stimulated-based model for oscillations in Ca^{2+} concentration. *Proc. Natl. Acad. Sci. USA*. 89:9895–9899.
28. Parker, I., and I. Ivorra. 1990. Inhibition by Ca^{2+} of inositol trisphosphate-mediated Ca^{2+} liberation: a possible mechanism for oscillatory release of Ca^{2+}. *Proc. Natl. Acad. Sci. USA*. 87:260–264.
29. Mak, D. O., S. McBride, and J. K. Foskett. 2001. ATP-dependent adenophostin activation of inositol 1,4,5-trisphosphate receptor channel gating. *J. Gen. Physiol.* 117:299–314.
30. Bezprozvanny, I., and B. E. Ehrlich. 1994. Inositol (1,4,5)-trisphosphate (InsP3)-gated Ca channels from cerebellum: conduction properties for divalent cations and regulation by intraluminal calcium. *J. Gen. Physiol.* 104:821–856.
31. Parker, I., and I. Ivorra. 1992. Characteristics of membrane currents evoked by photoreleased inositol trisphosphate in *Xenopus* oocytes. *Am. J. Physiol.* 263:C154–C165.